ELSEVIER

Catalysis Today 41 (1998) 179–189

CATALYSIS TODAY

Microcalorimetric characterisation of acid–basic catalysts

Vincenzo Solinas*, Italo Ferino

Dipartimento di Scienze Chimiche, Via Ospedale 72, 09126 Cagliari, Italy

Abstract

Fundamentals of microcalorimetry are briefly reviewed. A heat-flow microcalorimeter of the Tian–Calvet type has been used to obtain information on the differential molar enthalpy of adsorption. Ammonia, pyridine, *n*-butylamine or CO_2 and SO_2 have been used to characterize the acid–base properties of several catalysts such as zeolites and oxides. © 1998 Elsevier Science B.V. All rights reserved.

Keywords: Calorimetry; Acid-basic catalysts

1. Fundamentals of calorimetric technique

The surface properties of a solid are of primary importance in governing the energetics of the adsorption, reaction and desorption steps, which represent the core of a catalytic process. These properties can be conveniently investigated by studying the adsorption of suitably chosen probe molecules on the solid. Adsorption occurs at the interface between a fluid phase and a solid. The process is originated by the presence on the surface of coordinately unsaturated species able to interact with molecules from the gas phase, whose concentration at the interface results increased in comparison with that in the bulk gas phase.

The solid is called the adsorbent and the adsorbed substance the adsorbate. According to the relationship:

$$\Delta G_{ads} = \Delta H_{ads} - T\Delta S_{ads}, \quad (1)$$

adsorption is generally exothermic ($\Delta H_{ads}<0$), as it occurs spontaneously ($\Delta G_{ads}<0$) and leads to a more ordered state ($\Delta S_{ads}<0$).

The heat evolved is called the heat of adsorption and can be measured experimentally. It is related to the energy of the bonds formed and thus represents a measure of the strength of the interaction. The accurate measurements of the heat evolved and the amounts adsorbed are difficult. In order to detect energetic heterogeneity of the surface, which is of primary interest in catalysis, small doses of probe gas (typically <10 μmol g^{-1} of catalyst) have to be admitted successively on the solid, in order to saturate the active sites progressively. Corresponding heats range from 100 up to 1000 mJ and require a few hours for being evolved. Since the development of commercial instrumentation able to measure quantitatively such low heats and adsorbed amounts, microcalorimetry has gained importance as one of the most reliable methods for the study of gas–solid interactions.

Most commonly used are heat-flow microcalorimeters of the Tian–Calvet type. The detailed theory and operation of this calorimeter can be found in [1]. The apparatus is composed by an experimental vessel,

*Corresponding author.

PII S0920-5861(98)00048-0

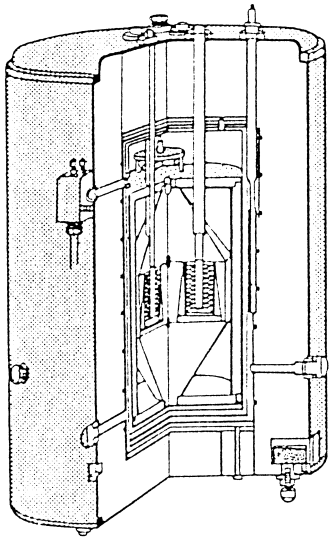

Fig. 1. Calvet microcalorimeter.

where the system is located, which is contained into a calorimetric block (Fig. 1). The temperature of the block, which works as a heat sink, is controlled very precisely. The heat generated in the system flows to the heat sink and is accurately measured by means of a detector. This is made up of a large number of identical conductive thermocouples (a thermopile) that surround the vessel and connect it to the block (Fig. 2)

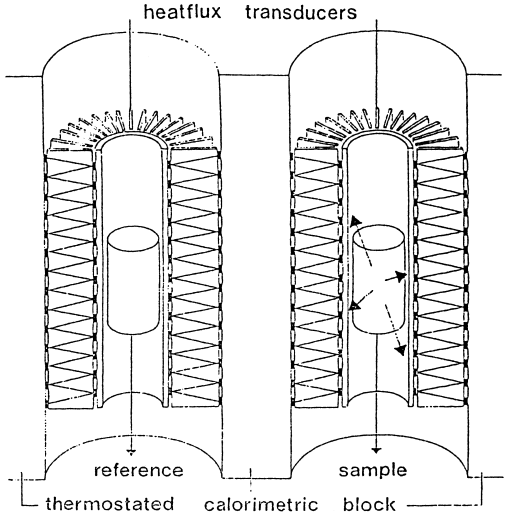

Fig. 2. Thermostated calorimetric block.

in such a way that the vessel and the block temperatures are always close to each other. A signal is generated by the detector that is proportional to the heat transferred per unit time. Undesired signals due to external temperature fluctuations in the calorimetric block are minimized by connecting in opposition two heat-flow detectors from two identical vessels, one of which is used to perform the experiment, the other being used as a reference. Heat related to the introduction of the probe and other parasitic phenomena are thus compensated.

The heat generated by the sample inside the vessel is transferred completely through the thermocouples, provided that radiation, conduction along the wall of the vessel, conduction and convection through the fluid phase are minimized by the design of the apparatus. A voltage signal, E, is generated by the thermocouples and recorded over the time of the thermal event, whose end is indicated by the returning of the thermopile output signal to the base line. The total heat produced during the event is given by the area under the thermogram:

$$Q_{\text{exp.}} = K \int_{\text{exp.}} E \, \mathrm{d}t, \tag{2}$$

where K is the instrument constant [1].

This highly sensitive calorimeter needs to be connected to a sensitive volumetric system in order to determine accurately the amounts adsorbed. A schematic representation of the whole assembly is shown in Fig. 3. The measure section, where the pressure measuring device is located, is between V_0 and V_1. The vessels section which contains the calorimeter, is between V_0 and V_2. The experiments are carried out isothermally by admitting stepwise increasing doses of the probe gas or vapor to the solid, previously evacuated at 10^{-6} Torr. The heat evolved by each dose is measured and the corresponding amount adsorbed is obtained by the pressure drop in the known volume of the apparatus. This is determined in previous calibration by allowing a known amount of gas to expand from the measure section into the vessels section (formerly evacuated). For each dose thermal equilibrium must be attained before the pressure p_i, the adsorbed amount $\Delta n_{\text{a},i}$ and the integral heat evolved $\Delta Q_{\text{int.},i}$ are measured. The adsorption experiment is concluded when a relatively high pressure is

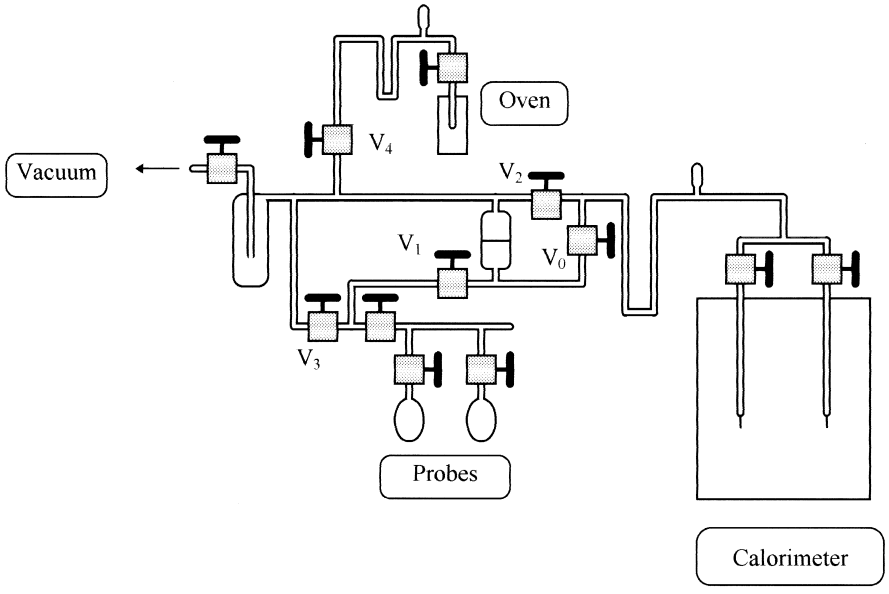

Fig. 3. Microcalorimetric apparatus.

reached without significant evolution of heat and the adsorbed amount becomes negligible.

From the above data the equilibrium pressure, P, the amount adsorbed up to the ith dose, $\sum \Delta n_{a,i}=n_a$, and the corresponding heat evolved, $\sum \Delta Q_{int.,i}=Q_{int.}$ are obtained. The results are presented in terms of a volumetric isotherm (n_a vs. P, Fig. 4 (A), curve 1) and a calorimetric isotherm ($Q_{int.}$ vs. P, Fig. 4(B), curve 1). After evacuation, readsorption can be carried out on the same sample, giving isotherms corresponding to the reversible adsorption only (Fig. 4(A) and (B), curves 2). From the reversible volumetric and calorimetric isotherms computation of the thermodynamic functions (energy and entropy of adsorption) can be undertaken, according to Cardona-Martinez and Dumesic [2].

Integral heat is often plotted as a function of coverage ($Q_{int.}$ vs. n_a), as shown in Fig. 5. This allows to reveal regions of constant heat of adsorption, where the heat evolved is linearly dependent on coverage.

Most commonly, adsorption microcalorimetry is devoted to the determination of the site energy distribution. This is usually done by representing the differential heat of adsorption as a function of coverage. The differential heat of adsorption, $q_{diff.}$, is related to the integral heat of adsorption, $Q_{int.}$, by:

$$q_{diff.} = [\vartheta Q_{int.}/\vartheta n_a]T, m, \quad (3)$$

where m is the mass of solid.

It can be shown [2] that for a Tian–Calvet calorimeter, where all the other effects are compensated, it represents the differential molar enthalpy of adsorp-

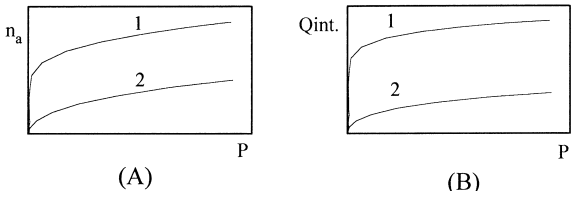

Fig. 4. Volumetric isotherms (A) and calorimetric isotherms (B).

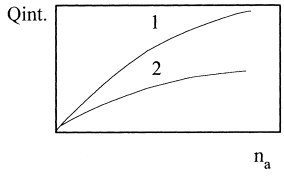

Fig. 5. Integral heat vs. adsorbed amount.

tion. The curves, $q_{\text{diff.}}$ vs. n_a, can be obtained from the calorimetric experiments as follows: a histogram is constructed, where the evolved heat divided by the number of moles adsorbed from the admitted dose ($\Delta Q_{\text{int.}}/\Delta n_{a,i}$) is reported vs. n_a; a continuous curve is then traced through the points located on the abscissa at the center of the corresponding increment. Alternatively, an analytical function can be used to fit the integral heats accumulated for the successive increments, which is then differentiated with respect to the amount adsorbed to obtain the differential heats. Thus, if a polynomial of the form:

$$Q_{\text{int.}} = \sum_k a_k n_a^k \tag{4}$$

is used to fit by least squares the integral heat curve (a_k being the fitted coefficients), the differential heat is:

$$q_{\text{diff.}} = \mathrm{d}Q_{\text{int}}/\mathrm{d}n_a = \sum_k k a_k n_a^{k-1}. \tag{5}$$

The decrease of differential heat with coverage is usually ascribed to the heterogeneity of the adsorption sites. In Fig. 6 generalized types of $q_{\text{diff.}}$ vs. n_a curves are shown [3]. The presence of well-defined steps as in curve A, is taken as an indication of discrete inhomogeneity, i.e. different "families" of sites are present, each family with a characteristic value of $q_{\text{diff.}}$. The sites with the highest $q_{\text{diff.}}$, i.e. the strongest in terms of energy of interaction with the probe molecules, are occupied first and this corresponds to plateau 1. Once the sites of this family are saturated, adsorption continues on the family of sites with immediate lower energy (plateau 2) and so on. Curve B shows a continuous decrease of $q_{\text{diff.}}$ at low coverage (region 1 of the curve) which points out to the presence on the sample of strong sites not belonging to a same family. Once these sites are saturated, a plateau is observed (region 2) corresponding to homogeneous sites forming a family of constant $q_{\text{diff.}}$. Continuous heterogeneity is observed again in region 3 of curve B. Curve C refers to a sample whose sites do not form any family of characteristic heat, i.e. continuous heterogeneity is observed at any coverage. It must be emphasized that the above $q_{\text{diff.}}$ vs. n_a curves represent true site distribution only in the case when the adsorption is not limited by kinetic processes. In the following this aspect will be briefly considered. A detailed treatment of the subject can be found in [2].

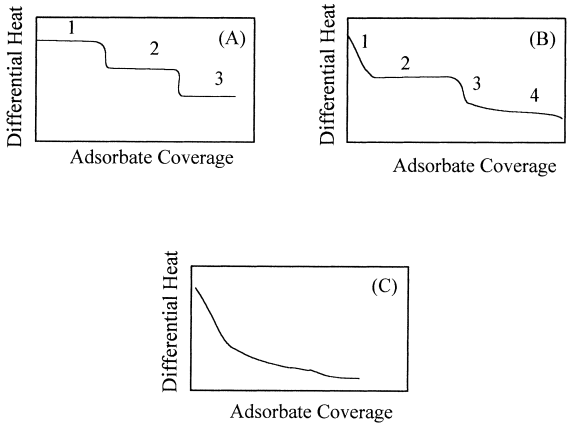

Fig. 6. Types of thermograms in isothermal adsorption.

Assuming a concentration of active sites of 2×10^{17} sites m^{-2}, a gas pressure of 1 Torr and an activation energy of 20 kJ mol^{-1}, the initial adsorption rate at 473 K has been estimated [2] to be so fast that covering of the surface requires no more than a few seconds, i.e. a time well below the timescale of the calorimetric experiment. Concerning desorption, the rate constant is:

$$k_{\text{des.}} = A_{\text{des}} \exp - [Ea_{\text{des}}/RT]. \tag{6}$$

The activation energy for desorption is related to that for adsorption through the following relationship:

$$Ea_{\text{des}} = q_{\text{ads}} + Ea_{\text{ads}}. \tag{7}$$

That is, the rate of desorption per molecule adsorbed depends on the heat of adsorption, which thus determines the time needed for the establishing of equilibria with the gas phase. It has been estimated [2] that at 473 K equilibrium can be reached during the timescale of the experiment only when q_{ads} does not exceed 140 kJ mol^{-1}. If the calorimetric experiment is performed at 473 K and a distribution of sites exists on the surface with sites of q_{ads} higher than 140 kJ mol^{-1}, and the adsorbed molecules are immobile on the surface (i.e. they stay adsorbed on the sites they are first adsorbed) the true site distribution is not obtained. The measured differential heat is then just an average value of the sites that the molecules adsorb on, and differences among sites are not detected.

However, the molecules which are adsorbed on different surface sites could move from one site to

another during their resident time on the surface (and spend more time on the stronger sites), provided that the activation energies for diffusion along the surface are lower than those for desorption. If the thermal energy is high enough that equilibration among the molecules in different surface sites is attained during the timescale of the experiment, true site distribution is obtained. Reasonable assumptions for the parameters involved in the diffusional process allow to conclude [2] that at 473 K true site distribution can be obtained for q_{ads} up to 240 kJ mol^{-1}. The threshold value depends on temperature, being lower for lower temperatures of the experiment. Therefore, in order to be confident of detecting time differences among the sites of a heterogeneous surface (i.e. $q_{diff.}$ vs. n_a curves corresponding to thermodynamically stable site occupation) one has to perform experiments at as high a temperature as possible, compatible with a favorable adsorption equilibrium constant and the thermal stability of the adsorbate.

In the case of a surface with discrete sites (curve A in Fig. 6) an equation based on Langmuir's model has been proposed [4] for describing the dependence of the differential heat on the adsorbed amount.

Considering a species A adsorbing on a homogeneous surface and denoting by σ the surface site we have:

$$A_{(g)} + \sigma \underset{k_{-1}}{\overset{k_1}{\rightleftarrows}} A\sigma.$$

The corresponding Langmuir's isotherm [5] is:

$$\Theta = \frac{Kp}{1 + Kp}, \tag{8}$$

where $K{=}k_1/k_{-1}$ represents the equilibrium constant for adsorption and θ is the coverage, i.e. the ratio between the amount adsorbed, n, and the amount required for the complete formation of a monolayer, n_m.

If S different families of sites are present the coverage is obtained by adding the coverages for each family of sites:

$$\Theta = \sum_{i=1}^{S} \Theta_i = \sum_{i=1}^{S} \frac{X_i K_i p}{1 + K_i p} = \sum_{i=1}^{S} \frac{n_i}{n_m}, \tag{9}$$

where X_i is the fraction of centers i, n_i is the amount adsorbed on sites of the ith family and n_m is the maximum adsorption capacity. Successive filling of the different types of sites occurs if the equilibrium constants are largely different. At equilibrium the amount n is distributed among all the families of sites. According to Cardona-Martinez and Dumesic [2], the total amount, n, is obtained as a function of the amount adsorbed on sites 1:

$$n = \sum_{i=1}^{S} n_i = \sum_{i=1}^{S} \frac{n_1 n_{im}}{n_{1m}\alpha_{1,i} - n_1(\alpha_{1,i} - 1)}, \tag{10}$$

where $\alpha_{1,i}{=}K_1/K_i$ is the selectivity or distribution coefficient. It is related to the entropies of adsorption for sites 1 and i.

The integral heat of adsorption, Q is related to the differential heats of adsorption of each family, q_i, by:

$$Q = \sum_{i=1}^{S} q_i n_i = \sum_{i=1}^{S} \frac{n_1 n_{im} q_i}{n_{1m}\alpha_{1,i} - n_1(\alpha_{1,i} - 1)} \tag{11}$$

and

$$q = \frac{dQ}{dn} = \frac{\sum^{S} q_i n_i \alpha_{1,i} / [n_{1m}\alpha_{1,i} - n_1(\alpha_{1,i} - 1)]^2}{\sum_{i=1} n_{im}\alpha_{1,i} / [n_{1m}\alpha_{1,i} - n_1(\alpha_{1,i} - 1)]^2}. \tag{12}$$

Accordingly, the experimental data can be fitted to obtain values for n_{im}, q_i and $\alpha_{1,i}$.

A decreasing trend without steps of $q_{diff.}$ vs. n_a (curve C or region 3 in curve B in Fig. 6) points out to the lack of families of sites of characteristic heat. In the case that this trend is linear it could be assumed that the sites have uniform inhomogeneity. For these sites, where

$$q_i = q_{0,i} - b_i n_i, \tag{13}$$

the adsorption isotherm is described by a logarithmic equation. The Themkin isotherm [6] is a special case of this situation.

A useful presentation of the results is based on the plot of the site energy distribution function vs. $q_{diff.}$. The site energy distribution function is the negative inverse of the first derivative of the differential heat with respect to the amount adsorbed, $-dn_A/dq_{diff.}$. Peaks will appear in this plot in correspondence with eventual steps in the $q_{diff.}$ vs. n_a curve. The area under each peak is proportional to the amount adsorbed on the family of sites whose strength corresponds to the

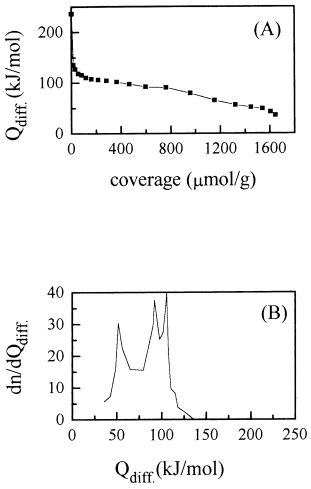

Fig. 7. Differential heat vs. adsorbed amount (A) and site strength distribution (B).

abscissa of the maximum. This allows easy comparison between catalysts. An example is presented in Fig. 7.

In the case that a polynomial function (Eq. (4)) is used to fit the experimental curve of integral heat, we get the site energy distribution function as:

$$-\frac{\mathrm{d}n_{\mathrm{a}}}{\mathrm{d}q_{\mathrm{diff.}}} = \left\{ -\sum_{k} k(k-1)a_k n^{k-2} \right\}^{-1}. \qquad (14)$$

The thermogram of each dose contains information about the kinetics of the adsorption.

Fast and slow processes can be distinguished (Fig. 8 (A)) and half-reaction times can be calculated for each dose (Fig. 8(B)). Kinetic data can be obtained [7] from the evolution of heat as a function of time (% $Q_{\mathrm{int.}}$ vs. time, Fig. 8(C)). The trend in pressure drop of the gas (Fig. 8(D)) is related to the kinetics of the process. This can be used, for slow processes, to speculate on the rate determining step by comparing t_{e}, the time needed to reach equilibrium, with t_0, the time required for the calorimetric signal t_0 to reach the baseline. If $t_{\mathrm{e}} \approx t_0$, the rate determining step should be an activated adsorption, whereas if $t_{\mathrm{e}} \ll t_0$ a rapid adsorption is followed by slow surface reactions [8]. However, the exploitation of the kinetic information contained in the thermogram has been attempted by just few authors owing to difficulties arising from thermal lag phenomenon.

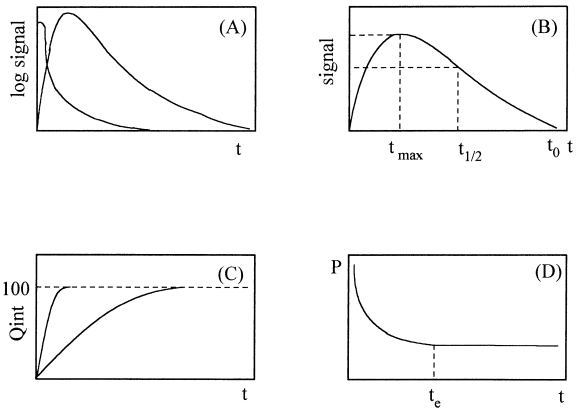

Fig. 8. Thermograms and thermokinetic parameters.

2. Acid–base properties of catalyst surfaces

The measurement of the acidity of solid acid surfaces has been the aim of many studies. The techniques used are Hammet titrations, chemisorption of bases, IR spectroscopy and TPD [9–12].

In most recent calorimetric studies of the acid–base properties of surfaces ammonia, pyridine, *n*-butylamine, triethylamine, or other basic molecules have been used to characterize the surface acidity. In some experiments, acidic probe molecules such as CO_2, SO_2 or hexafluoroisopropanol have been used to characterize the surface basicity of some solids.

Heats of adsorption of the probe molecules have been frequently measured near to room temperature, but these measurements may not give accurate quantitative results owing to nonspecific adsorption. Furthermore, the temperature of the experiment could be too low for allowing detection of differences among the sites, the measured differential heat then being just an average value.

Zeolites offer a wide range of catalytic applicability in the chemical industry. They are usually synthesized in the sodium form and the sodium ions can be exchanged with other cations. The zeolite also can be treated with ammonium ions to exchange the sodium. An ammonium zeolite on heating loses ammonia and it is said to be decationed.

The acidity and acid strength of a zeolite can be modified by changing the sample pretreatment or preparation method, by exchanging the cations or by modifying the Si/Al ratio. The knowledge of the

influence of these parameters allows to control them; thus if, for instance, excessive polymerization is to be avoided but high conversion is necessary, then very strong acid sites must be avoided, though a large total acidity is still required.

The activation temperature can influence the acid strength distribution. The differential heat of NH_3 adsorption at 423 K for a HY zeolite indicated that stronger acid sites in the range 150–180 kJ mol^{-1} were formed upon increasing the activation temperature from 573 to 923 K [13,14].

Dehydroxylation at high temperature results in strong Lewis acid sites formation, and the disappearance of intermediate and weak Brønsted sites. The presence of nonframework aluminium is also evidenced. Stepwise adsorption of ammonia at 573 K [15] showed that ammonia reacts first with the Lewis acid sites, and then with Brønsted sites and finally with terminal Si-OH groups.

IR studies show that the strongest sites (170 kJ mol^{-1}) on dehydroxylated zeolites are Lewis acid sites and that ammonia adsorption is dissociative on these sites, while the heats of 100 kJ mol^{-1} characterize adsorption on Lewis acid sites without dissociation [16].

Adsorption of NH_3 on Brønsted acid sites produced heats in the range 100–150 kJ mol^{-1} for several zeolites at 573 K.

Results at 303 K indicate that NaY zeolites are weakly acidic with heats of adsorption of 94 kJ mol^{-1} for ammonia and 124 kJ mol^{-1} for pyridine [17]. This zeolite also presents weak basic sites, 40 kJ mol^{-1}, by adsorption of CO_2 at 298 K [18].

An important effect is associated to the total or partial exchange of NaY to give NaHY zeolite. The initial heat of *n*-butylamine adsorption at 303 K increases, with increase in the degree of H exchange, from 105 to 158 kJ mol^{-1} and the strength of intermediate sites increases from 110 to 158 kJ mol^{-1} [19,20].

Zeolites can be dealuminated using different procedures such as extraction with EDTA, high temperature steaming, reaction with $SiCl_4$, or substitution with $(NH_4)_2$ SiF_6. These procedures can be followed by acid leaching to remove the nonframework aluminium.

Steam dealumination of HY zeolite at high temperature causes a progressive destruction of weak intermediate sites and produces new stronger sites [14]. During this process mesopores are formed throughout a well-ordered silica framework.

Dealumination by $SiCl_4$ leads to zeolites having an increased Si/Al ratio with good crystallinity and with less presence of extraframework aluminium [21].

Dealumination of zeolites by isomorphous substitution with $(NH_4)_2$ SiF_6 leads to catalysts free of extraframework cationic species and with a much higher acidity than conventionally dealuminated solids with similar Si/Al ratios [19].

Generally, the strength of the strong Brønsted sites increases with the dealumination level; a maximum in overall acidity is achieved at Si/Al ratio of 7 for HY zeolites.

Dealumination or dehydroxylation at elevated temperatures produces strong Lewis acid sites at the expense of Brønsted sites.

The dehydroxylated samples undergo an irreversible transformation while the dealuminated samples can recover a part of the acidity by acid leaching.

The changes in the acid strength distribution are manifested as changes in catalytic behavior. The dealumination of HY zeolites increases the catalytic activity for cumene cracking at 573 K, reaching a maximum at a Si/Al ratio of about 7.4. Further removal of Al reduces both the catalytic activity and the acidity of the catalysts [23,24]. In the cracking reaction of cumene carbenium ions are believed to be formed on the Brønsted acid sites of the catalyst [11]. A site having stronger acidity should show higher activity for the formation of carbenium ion and consequently show a higher cracking ability. The increase in catalytic activity at a low degree of dealumination seems to be due to the elimination of weak acid sites and an increase in the concentration of the stronger Brønsted sites associated with the residual Al atoms. Dealumination seems to convert some of the rings containing two or more Al atoms into rings containing a single AlO_4 tetrahedron, thus increasing the number of strong acid sites. The calorimetric results obtained at 298 K do not correlate with the catalytic activity at 573 K but the cracking activity agrees better with the acidity determined by adsorption of puridine at 473 K. Thus, when attempting to correlate the activity for an acid reaction with the surface acidity, it is important to study the adsorption process at the temperature used for the catalytic reaction, and the basic molecule used should have a similar size to that of the reactants.

The acid–base properties of sodium form of ZSM-5 zeolites [18] have been studied by adsorption of ammonia at 416 K and of CO_2 at 293 K. This zeolite presents only few weak acid and basic sites.

The acid–base properties of alkali-metal ion-exchanged X and Y zeolites were investigated by ammonia and sulfur dioxide adsorption microcalorimetry [25]. Li and Na zeolites present much higher heats of NH_3 adsorption and greater coverage at the same pressure than the other zeolites. The acidity strength of X differs by only a few kJ mol^{-1} from the corresponding Y zeolites. The amounts of SO_2 adsorbed are very similar for all the Y zeolites except for LiY, on which the amount is smaller. X zeolites adsorb higher amounts than Y zeolites. Most of the samples have centers possessing significant basicity (Q>150 kJ mol^{-1}). Microcalorimetric measurements on Cs-exchanged X containing excess cesium oxide indicated that the extra framework cesium oxide provided even stronger basic adsorption sites. Calorimetric results were correlated with the general physicochemical parameters; intermediate electronegativity of the zeolite structure, the charge to radius ratio of the cation, and the partial oxygen charge.

Less work has been performed to characterize the acidic and basic sites of oxides. Silica shows low heats of adsorption for both basic molecules (ammonia, *n*-butylamine, pyridine) and acidic molecules (hexafluoroisopropanol) indicating that the surface sites on silica are both weakly acidic and basic. The adsorption is mainly due to hydrogen bonding and Van der Waals interaction; more than 98% of the pyridine adsorbed at 423 K was hydrogen bonded [22]. The differential heats of ammonia on silica [18] show a decrease as the adsorption temperature increases.

The differential heats of adsorption of ammonia [18,23,26] or carbon dioxide [18,26] on the surface of alumina, show the presence of strong acid sites and basic sites, respectively. The heat of adsorption for alumina is typical of a strong acidic surface; the initial heat increases and the adsorption capacity decreases with increasing adsorption temperature. The silica–alumina surface shows a behavior similar to the zeolites for the initial differential heats of ammonia and pyridine, but the total number of acidic sites is smaller. The basicity of silica–alumina surface, determined by CO_2 [18,26], appears to be weaker than that on pure alumina.

Adsorption microcalorimetry of pyridine of 473 K has been used to determine the distribution of acidic strength of silica-supported oxides [27,28]. The acidic strength distributions showed several regions of constant heat, while silica had homogeneous surface sites. The Ga, Al and Sc supported oxides were found to have both Brønsted and Lewis acidity, whereas the Zn, Fe and Mg samples showed only Lewis acidity. The highest heats of pyridine adsorption over these catalysts are due to strong Lewis acidity whereas intermediate heats were attributed to weaker Lewis acid sites or a combination of Lewis and Brønsted acid sites. These results are confirmed by using IR spectroscopy of adsorbed pyridine [29]. The authors studied the activity of isopropanol dehydration over these catalysts and they found that samples showing only Lewis acidity were at least one to two orders of magnitude less active than the samples that displayed Brønsted acidity. The activity of these samples increased in the order Al>Ga>Sc. This is the same order found for differential heats of pyridine adsorption on the Brønsted acid sites.

The differential heats of adsorption of NH_3 and CO_2 over 18 oxides were determined [30,31]. These oxides were classified, according to their properties, as acidic oxides: Cr_2O_3, WO_3, Nb_2O_5, V_2O_5/SiO_2 and MoO_3; amphoteric oxides: BeO, TiO_2, Al_2O_3, ZnO_2, and ZnO; and basic oxides: ThO_2, Nd_2O_3, MgO, CaO and La_2O_3. It was found that many oxides in the amphoteric group adsorbed more NH_3 and with a higher heat (>200 kJ mol^{-1}) than some of the ones in the acidic group. Also the ZrO_2 sample adsorbed NH_3 with a heat of 150 kJ mol^{-1}, comparable to Nb_2O_5 and WO_3. The group of basic sites adsorbed NH_3 very weakly (<20 kJ mol^{-1}) essentially owing to physisorption. The oxides of La, Nd and Th adsorbed CO_2 in larger abundance and higher heat, for instance 200 kJ mol^{-1} for Nd, than other oxides. It is worth noting that, on the alkaline earth oxides, the heat of adsorption of CO_2 were only 120–16O kJ mol^{-1}, perhaps due to bidentate adsorption of CO_2. TiO_2, ZrO_2 and Al_2O_3 also adsorbed CO_2 with heats of adsorption of 100 kJ mol^{-1}, but with an amount smaller than on the basic oxides.

A later study [32] examined the NH_3 and CO_2 adsorption heats on several zirconia catalysts, differ-

ing in their preparative procedures and/or in the addition of dopants. These catalysts were used to produce alk-1-ene from 4-methylpentan-2-ol. The alcohol was found to undergo dehydration, giving 4-methylpent-1-ene and 4-methylpent-2-ene in variable amounts; skeletal isomers of C_6-alkenes were also formed in some cases. Simultaneous dehydrogenation was shown by 4-methylpenten-2-one formation. A cooperative action of acid and base sites is thought to operate when secondary alcohols are reacted on metal oxides. Three mechanisms are usually considered: E1, E2 and E1cB; these mechanisms should be regarded as limiting cases and intermediate situations can occur, particularly with the E1 and E2 mechanisms. The shift in the reaction pathway is influenced by the nature and strength of the sites; the Hofmann orientation and ketone formation are generally associated with a higher basicity of the catalyst.

Thus, the acid–base properties of zirconia should be involved in the catalysis of the dehydration reaction. The differential heats of ammonia and CO_2 adsorption are shown in Fig. 9. Initial heats of NH_3 fall within the range 210–85 kJ mol^{-1} and the shape of the heats vs. coverage curves represents all the possible situations (Fig. 9(A)). A few samples possess different types of sites; each type adsorbs the probe molecule with characteristic value of heat adsorption (140, 130, 120 kJ mol^{-1}). Other samples exhibit sites of specific heat of adsorption as well as sites with a continuous variation of heat. Three of the samples show a continuous adsorption heterogeneity. The differential heats of adsorption of CO_2 on the same samples also show a wide range of variability (Fig. 9(B)). The ratio between the number of the basic and acidic sites, n_B/n_A, has been calculated for each catalyst from the microcalorimetry results, by dividing the amount of adsorbed CO_2 by the amount of adsorbed NH_3. The fraction of acid sites showing a differential adsorption heat of ammonia greater than 100 kJ mol^{-1} and the fraction of basic sites with a differential adsorption heat of CO_2 greater than 100 kJ mol^{-1} have also been calculated.

Fig. 10 shows that alk-1-ene selectivity increases with n_B/n_A, reaches a maximum and then decreases, whereas ketone formation continuously increases, being negligible for low n_B/n_A values. For the catalysts in the left-hand side of Fig. 10 the prevalence of the E1 mechanism seems rather likely. The triggering of

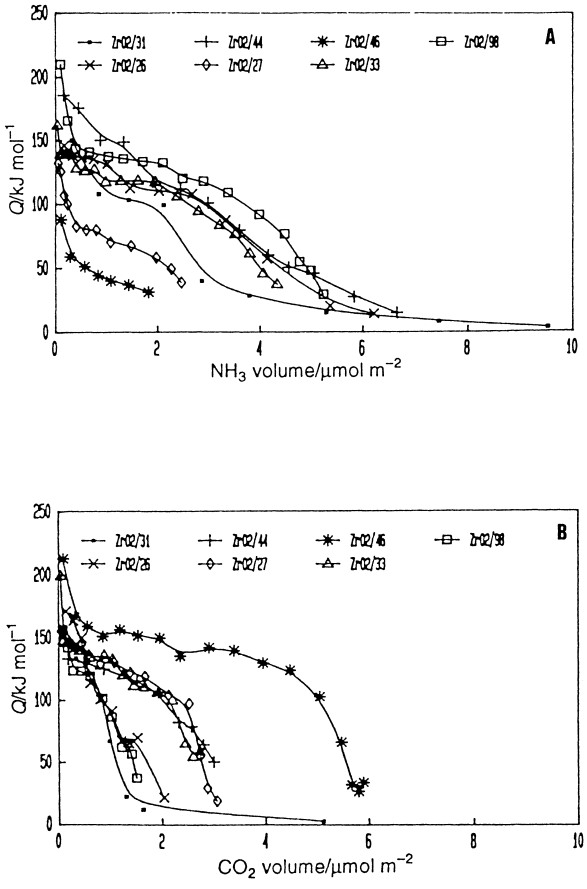

Fig. 9. Differential heats of adsorption of NH_3 (A) and CO_2 (B) as a function of coverage for zirconium oxides (reprinted with kind permission from [32]).

the process by attack of the acid site on the hydroxy group of the alcohol is favored by the lower n_B/n_A values. The ratio of C_6 skeletal isomers to 4-methylpenten-2-ene is the highest for the sample with the highest fraction of sites stronger than 100 kJ mol^{-1}. The maximum for alk-1-ene selectivity occurs at n_B/n_A=1.2. This represents a situation where the acid and base functions are well balanced, in terms of site numbers, and allow a two-point adsorption. The oxygen of the OH group of the alcohol interacts with a surface acid center, while a basic site interacts with the more acidic β-hydrogen, i.e. that of the methyl group. At the same time, most of the basic sites are strong enough to determine the C–H bond rupture first, which leads to carbanion formation and the establishing of

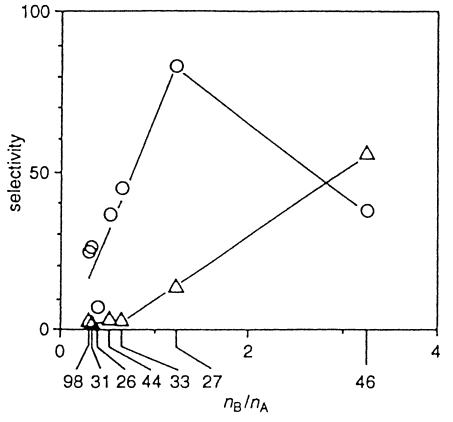

Fig. 10. Selectivity to 4-methylpent-1-ene (circles) and 4-methylpentan-2-one (triangles) vs. n_B/n_A for zirconia catalysts (reprinted with kind permission from [32]).

the E1cB mechanism. At high n_B/n_A values the lack of acid centers makes the adsorption of the alcohol through the two-point mechanism unlikely. A basic site (surface oxygen anion) can however interact with the OH group of the alcohol by means of a hydrogen bond. The weakening of the Cα-H bond favors the interaction of Hα with a positively polarized H atom (originating from the previously split O–H group of the alcohol) and the formation of a hydrogen molecule. Thus, a situation where the number of acid sites is lower than that of the base sites and most of the latter are strong limits dehydration, but allows dehydrogenation.

Further investigation on the conversion of 4-methylpentan-2-ol over lanthanum and cerium oxides [33] confirmed these findings, as shown in Fig. 11, allowing to conclude that a well-balanced number of acid and base sites is needed to obtain a good selectivity to the alk-1-ene isomer. Furthermore, the conversion of 4-methylpentan-2-ol seems a suitable reaction for exploring possible correlations between the catalytic behavior and the acid–base properties of catalysts [25].

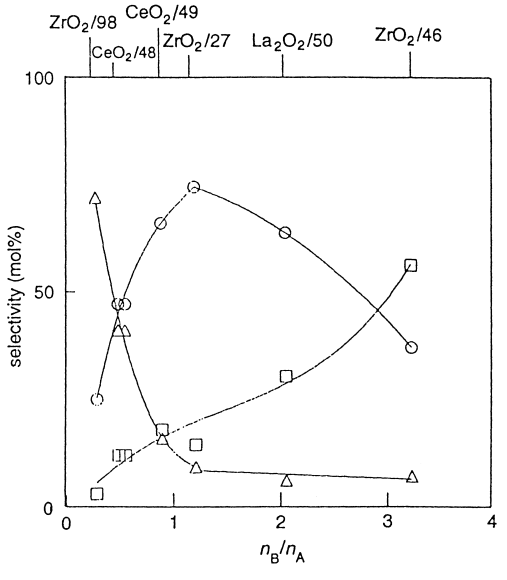

Fig. 11. Selectivity to 4-methylpent-1-ene (circles), alk-2-enes (triangles) and 4-methylpentan-2-one (squares) vs. n_A/n_B for lanthanum, cerium and zirconium oxides (reprinted with kind permission from [33]).

References

[1] A. Auroux, in: Les techniques physique d'etude des catalyseurs, Editions Technip., 1988, p. 823.
[2] N. Cardona-Martinez, J.A. Dumesic, in: Advances in Catalysis, vol. 38, Academic Press, New York, 1992, p. 149.
[3] P.J. Andersen, H.H. King (Eds.), in: Catalysis, vol. 11, Royal Society of Chemistry, Cambridge, 1994, p. 441.
[4] A.L. Klyachko, Kinet. Katal. 19 (1978) 1218.
[5] I. Langmuir, J. Am. Chem. Soc. 40 (1918) 1361.
[6] G.A. Somorjai, Priciples of Surface Chemistry, Prentice-Hall, Englewood Cliffs, NJ, 1972.
[7] T.L. Hill, J. Chem. Phys. 18 (1950) 246.
[8] T.L. Hill, Adv. Catal. 4 (1952) 212.
[9] K. Tanabe, in: J.R. Anderson, M. Boudart (Eds.), Catalysis: Science and Technology, vol. 2, Springer, New York, 1981, p. 231.
[10] H. Knözinger, Adv. Catal. 25 (1976) 184.
[11] H.A. Benesi, B.H. Winquist, Adv. Catal. 27 (1978) 98.
[12] D. Barthomeuf, in: B. Imelik, C. Naccache, G. Coudurier, Y.B. Taarit, J.C. Vedrine (Eds.), Catalysis by Acids and Bases, Elsevier, Amsterdam, 1985, p. 75.
[13] R.D. Shannon, K.H. Gardner, R.H. Staley, G. Bergeret, P. Gallezot, A. Auroux, J. Phys. Chem. 89 (1985) 4778.
[14] A. Auroux, Y.B. Taarit, Thermochim. Acta 122 (1987) 63.
[15] G.I. Kapustin, L.M. Kustov, G.O. Glonti, T.R. Brueva, V. Borovkov, A.L.Y. Klyachko, A.M. Rubinstein, V.B. Kazanskii, Kinet. Katal. 25 (1984) 1129.
[16] A.L. AKlyachko, G.I. Kapustin, G.O. Glonti, T.R. Brueva, A.M. Rubinshtein, Zeolites 7 (1987) 119.
[17] A.L. Klyachko-Gurvich, T.R. Brueva, I.V. Mishin, G.L. Kapustin, A.M. Rubinstein, Acta Phys. Chem. 24 (1978) 183.
[18] A. Auroux, J.C. Vedrine, in: B. Imelik, C. Naccache, G. Coudurier, Y.B. Taarit, J.C. Vedrine (Eds.), Catalysis by Acid and Bases, Elsevier, Amsterdam, 1985, p. 311.

[19] T.R. Brueva, A.L. Klyachko, I.V. Mishin, A.M. Rubinshtein, Izv. Akad Nauk. SSSR, Ser Khim. 4 (1975) 939.
[20] A. Macedo, A. Auroux, F. Raatz, E. Jacquinot, R. Boulet, ACS Symp. Ser. 368 (1988) 98.
[21] Z.C. Shi, A. Auroux, Y.B. Taarit, Can. J. Chem. 66 (1988) 1013.
[22] G. Connell, Ph.D. Thesis, University of Wisconsin – Madison, 1985.
[23] K. Tsutsumi, H.Q. Koh, S. Hagiwara, H. Takahashi, Bull. Chem. Soc. Jpn. 48 (1975) 3576.
[24] I.V. Mishin, A.L. Klyachko-Gurvich, T.R. Brueva, A.M. Rubinshtein, Izv. Akad. Nauk. SSSR, Ser Khim. 8 (1979) 1739.
[25] A. Auroux, P. Artizzu, I. Ferino, R. Monaci, E. Rombi, V. Solinas, Microporous Mater., submitted.
[26] A. Auroux, A. Gervasini, J. Phys. Chem. 94 (1990) 6371.
[27] N. Cardona-Martinez, Ph.D. Thesis, University of Wisconsin – Madison, 1989.
[28] N. Cardona-Martinez, J.A. Dumesic, J. Catal. 127 (1991) 706.
[29] G. Connel, J.A. Dumesic, J. Catal. 105 (1987) 285.
[30] A. Auroux, A. Gervasini, J. Phys. Chem. 94 (1990) 6371.
[31] A. Gervasini, A. Auroux, J. Thermal Anal. 37 (1991) 1737.
[32] A. Auroux, P. Artizzu, I. Ferino, V. Solinas, G. Leofanti, M. Padovan, G. Messina, R. Mansani, J. Chem. Soc. Faraday Trans. 91 (1995) 3263.
[33] A. Auroux, P. Artizzu, I. Ferino, V. Solinas, G. Leofanti, M. Padovan, G. Messina, R. Mansani, J. Chem. Soc. Faraday Trans. 91 (1996) 2619.